

A Hydrodynamic and Transport Model for Ultrarelativistic Heavy Ion Collisions at RHIC and LHC Energies

Yu-Liang Yan¹, Yun Cheng², Dai-Mei Zhou², Bao-Guo Dong¹, Xu Cai², Ben-Hao Sa¹, and Laszlo P. Csernai^{3,4}

¹ *China Institute of Atomic Energy, P. O. Box 275 (10), 102413 Beijing, China*

² *Institute of Particle Physics, Huazhong Normal University, 430079 Wuhan, China*

³ *Department of Physics and Technology, University of Bergen, 5007, Bergen, Norway*

⁴ *MTA-KFKI Research Inst for Particle and Nuclear Physics, 1525 Budapest, Pf. 49, Hungary*

(Dated: June 13, 2021)

Combining the hydrodynamic model (Hydro code) and the transport model (PACIAE model), we present the Hydro-PACIAE hybrid model. We use the Hydro-PACIAE hybrid model to calculate Au+Au collisions at $\sqrt{s_{NN}}=130$ GeV and Pb+Pb collisions at $\sqrt{s_{NN}}=2.76$ TeV. The obtained pseudo-rapidity and transverse momentum distributions well reproduce the experimental data. This shows that the Hydro-PACIAE hybrid model is useful to describe the ultrarelativistic Heavy Ion Collisions at RHIC and LHC Energies. We used the hybrid model to calculate the elliptical flow for the Pb+Pb collisions at $\sqrt{s_{NN}}=2.76$ TeV. The v_2 values are bigger than the experimental data at high p_T , and will become bigger when the Hydro evolution time is longer. The results indicate that the selection of the transition hypersurface has significant effect on the observable quantities.

PACS numbers: 12.38.Mh, 25.75.-q, 25.75.Nq, 51.20.+d

I. INTRODUCTION

The nucleus-nucleus collisions at the Relativistic Heavy Ion Collider (RHIC) produced an initial hot and dense matter and this has been interpreted as a strongly coupled quark-gluon plasma (sQGP) [1–4]. The Large Hadron Collider (LHC) opens up opportunities to explore the quark gluon plasma (QGP) in a wider energy region. The hydrodynamic models are useful tools to describe the hot and dense matter generated in the early stage of ultrarelativistic heavy ion collisions. Here, interactions are strong and frequent, so that the microscopic models that assume binary collisions with free propagation of constituents between collisions have limited validity. The advantage of hydrodynamic models is that one can vary flexibly the dissipative properties and the equation of state (EoS) of the matter and test its consequences on the reaction dynamics and the outcome. On the other hand, the initial and final freeze-out (FO) stages of the reaction are outside the domain of applicability of the hydrodynamic model.

Microscopic models, e.g. the transport model PACIAE, are quite successful to describe the partonic and hadronic stages of the collision. Unfortunately, the transport models are usually restricted to binary collisions. Thus their validity is limited in the hot and dense matter especially when the QGP is generated. Furthermore, explaining the QGP phase transition between the hadronic and the partonic phase on a microscopic level is also an open issue that still has to be resolved.

Recently the so-called hybrid models, combining microscopic and macroscopic modules, have been developed. There are several hybrid models [5–9]. In this paper, we present a hybrid model, Hydro-PACIAE, which combines the hydrodynamic model (Hydro code) and the transport model (PACIAE model). The hybrid model connects the different stages of the reaction and each of

these are matched [10] appropriately. The initial state for hydrodynamic model is constructed based on the so-called Effective String Rope model [11, 12], and considering that the system is close to local equilibrium at high energies. The subsequent fluid dynamical model assumes a QGP fluid in local equilibrium. Then we consider a transition from the QGP fluid phase to the partonic/hadronic phase, which is described by a combination of a fluid dynamical (FD) and a particle transport model, PACIAE. Here we try to gain more insight into the principles, which may govern these processes.

We use the hybrid model, Hydro-PACIAE, first to simulate the final hadron distribution in pseudo-rapidity and transverse momentum, as well as comparing the model results with the experimental data for Au+Au collisions at $\sqrt{s_{NN}}=130$ GeV and Pb+Pb collisions at $\sqrt{s_{NN}}=2.76$ TeV. Then we use the hybrid model to calculate the elliptic flow in Pb+Pb collisions at $\sqrt{s_{NN}}=2.76$ TeV.

II. HYBRID MODEL DESCRIPTION

The most essential observables in ultrarelativistic heavy ion reactions [13] from the laboratory detector can help us to understand the properties of the dense and hot matter. In general, we expect to extract more information from experiments, both on the Equation of State (EoS) and the transport properties of matter [14, 15]. We have to apply a realistic and suitable description with fully 3+1 dimensional dynamical evolution at all stages of the reaction.

A. hydrodynamic Model for initialization in Hybrid model

The hydrodynamic stage is calculated by using the Particle In Cells (PIC) method [16], which uses a mesh of cells with smaller, Lagrangian fluid elements in them. The model assumes the MIT Bag Model equation of state and relativistic perfect fluid. The total number of so called “Marker particles” (which are the Lagrangian cells) is about 5 million, and their number remains a constant during a collision. Marker particles are defined to carry the same amount of conserved baryon charge, thus this charge is also exactly conserved by the method. Each cell of the calculational mesh contains a larger number of marker particles, placed in the mesh randomly. The marker particles move among the cells of the mesh during the fluid dynamical development. As we know, hydrodynamic models assuming phase and chemical equilibrium during all stages of the reaction cannot account for all observations in general. However, they provide an efficient way to describe the nearly perfect fluid phase of QGP. Then, we transform the fluid in the cells into a set of partons or hadrons, which are then described with the PACIAE model.

The quark-gluon fluid is assumed to have a small viscosity [14], especially in the vicinity of the critical point of the phase transition to/from hadronic matter [15]. This phase transition [17] has significant dynamical effect on the hadronization, that in local, fluid dynamical phase equilibrium takes a long time, which contradicts to observations. To avoid this time delay recently rapid transition scenarios are assumed, which can be handled well in the hybrid approach.

The 3+1 dimensional, relativistic FD model, we use to describe energetic heavy ion reactions, is well established and describes the measured collective flow phenomena well [18, 19]. In our Computational Fluid Dynamics (CFD) calculation the initial state model is based on expanding flux tubes or streaks [11, 12]. It is a system where the matter is stopped within each streak, while streaks expand independently of each other. Thus, this model is applicable streak by streak and the momentum of the streaks varies, especially for the peripheral streaks where the asymmetry between the projectile and target contribution to the participant matter is the biggest. So, the streaks at the projectile and target sides move in the beam (z -) direction with substantial velocity difference. In the initial state model [11, 12] the initial transverse velocity is zero for all fluid elements.

In the CFD simulations with the PIC solution method [18, 19], the equations of relativistic FD were solved for a perfect quark-gluon fluid. At the same time the numerical method, due to the finite grid resolution, led to dissipation and thus to entropy production, which was analyzed [20]. From the entropy production we could determine the corresponding “numerical viscosity”, and this was approximately the same as the estimated, low viscosity of the quark gluon plasma. To avoid double

counting, i.e. over counting, of viscous dissipation, we did not add additional viscous terms to our CFD model simulations.

In case of heavy ion reactions the flow is not stationary and the shear flow geometry is only present in the initial state. Later, due to the large pressure of QGP the plasma explodes and expands almost radially in a way that the final flow pattern at freeze out is close to spherical, somewhat elongated longitudinally and in the reaction plane ($\pm x$ -direction) due to the dominant elliptic flow.

B. Basic Description in PACIAE model

The PACIAE model [21–23] is a parton and hadron cascade model, which is based on PYTHIA [24]. The model consists of four stages: The parton initialization, which decomposes the fluid into partons; The post transition partonic state consists of quarks, anti-quarks, and gluons; Then, in the parton evolution stage, we are evaluating the total and the differential cross sections arising from the partonic evolution, which can be simulated by the Monte Carlo method until the parton-parton collisions are ceased; Finally, the partons reach the hadronization at the moment of freeze-out (FO). This is described by the phenomenological fragmentation model (String fragmentation) and the coalescence model [25, 26]. After hadronization, the rescattering produces the final hadrons, and we obtain a configuration of hadrons in the spatial and momentum coordinates after the hadronization. The detailed description for PACIAE is the following:

1. **PARTON INITIALIZATION:** In the case if we start directly from two colliding nuclei, an $A+A$ ($A+B$) collision is decomposed into binary nucleon-nucleon (NN) collisions based on the collision geometry, so that every collision time is calculated by assuming that the nucleons propagate along straight line trajectories and interact with the NN inelastic (total) cross sections. Then the initial NN collision-list is constructed from these NN collisions. A NN collision with the earliest collision time is selected from the collision list, and the final state of the collision is obtained by the PYTHIA model with string fragmentation switched-off. Afterwards the diquarks (anti-diquarks) are broken randomly into quark pairs (anti-quark pairs), and one obtains a configuration of quarks, anti-quarks, and gluons, beside a few hadronic remnants for a NN collision.
In case of the hybrid model, we generate partons from the fluid cells of the FD model at a transition hyper-surface. This is described later.
2. **PARTON EVOLUTION:** The evolution is made via parton rescattering, with $2 \rightarrow 2$, binary LO-pQCD differential cross sections [27]. Then the total and differential cross sections in the parton evolution

(parton rescattering) are simulated by the Monte Carlo method.

3. **HADRONIZATION:** The parton evolution stage is followed by the hadronization at the moment of partonic freeze-out. This means no more parton collisions. In the PACIAE model, the Lund string fragmentation model and phenomenological coalescence model are supplied for the hadronization of partons after rescattering. In case of the hybrid model the latter one is used.
4. After hadronization the rescattering among produced hadrons is dealt with the usual two-body collision model. Only the rescatterings among $\pi, K, p, n, \rho(\omega), \Delta, \Lambda, \Sigma, \Xi, \Omega, J/\Psi$ and their antiparticles are considered in the calculations. An isospin averaged parametrization formula is used for the hh cross section [28, 29]. We also provide an option for the constant total, elastic, and inelastic cross sections ($\sigma_{\text{tot}}^{NN} = 40$ mb, $\sigma_{\text{tot}}^{\pi N} = 25$ mb, $\sigma_{\text{tot}}^{KN} = 35$ mb, $\sigma_{\text{tot}}^{\pi\pi} = 10$ mb) and the assumed ratio of inelastic to total cross section of 0.85.

C. Connection of Stages in Hybrid Model

We present the connection of the hydrodynamic model and PACIAE model, as the transfer of the fluid cell by cell to partons, satisfying the conservation laws based on the assumption of the thermal equilibrium before and after the transition. The detailed steps are as follows:

(1) The hydrodynamic model, assumes a QGP fluid, with an EoS given by the MIT Bag model with massless quarks and gluons and a background field. Each Lagrangian fluid cell has a given baryon charge, which are rescaling the charge density in the cells of the mesh, $n(x, y, z)$. We may deal with the transition hyper-surface in 3 optional ways: The first case is the simplest assumption that transition takes place isochronously, *i.e.* at $t = \text{const.}$; The second case is that the transition happens on a hyperboloid, *i.e.* at $\tau = \sqrt{t^2 - \vec{r}^2} = \text{const.}$, where τ is the proper transition time from a space-time point. The third case is when the transition is described as a sudden change across a space-time hyper-surface, which hyper-surface is calculated based on a condition (e.g. a transition temperature), if the transition condition is known. To be simple, in this work, we choose the first case, in which the direction of the flow and normal vectors are everywhere the same, and they are perpendicular to the transition hyper-surface.

(2) We use the perfect relativistic fluid dynamical equations:

$$N^\mu_{;\mu} = 0 \quad \text{and} \quad T^{\mu\nu}_{;\mu} = 0.$$

where $u^\mu = (\gamma, \gamma\vec{v})$, and $w = e + P$, $T^{ik} = w\gamma^2 v_i v_k + P\delta_{ik}$. During the transition, the above dynamical equations can

be simplified as conservation laws:

$$[T^{\mu\nu} d\hat{\sigma}_\nu] = 0, \quad [N^\mu d\hat{\sigma}_\mu] = 0. \quad (1)$$

In our simulation, the above conservation laws have to be satisfied [10] and the examination of the increasing entropy should be done during the whole simulation. For example, baryon charge, N_i , and the energy, E_i , are calculated according to the formula for each cell on the transition hyper-surface:

$$N_i = V_{\text{cell}}^{LR} n_i = V_{\text{cell}}^{LR} N_i^\mu u_\mu, \quad (2)$$

$$E_i = V_{\text{cell}}^{LR} e_i = V_{\text{cell}}^{LR} u_\mu T_i^{\mu\nu} u_\nu. \quad (3)$$

where the index “ i ” runs over the different generated parton or hadron species. V_{cell}^{LR} is the volume of the cell in the local rest frame. u_μ is the post transition 4-velocity, $u^\mu = \gamma(1, \vec{v})$, and $u_\mu = \gamma(1, -\vec{v})$, where $\gamma = 1/\sqrt{1 - \vec{v}^2}$. \vec{v} is the 3-velocity of the fluid cell in the partonic or hadronic phase. Note that this velocity after the transition is not the same as the flow velocity of the QGP. The energy momentum tensor $T_i^{\mu\nu}$ includes the contribution of the particles with their kinetic energies. In the post transition stage, particles in partonic matter include quarks, anti-quarks and massless gluons. The details of this transition are described in the Appendix V.

(3) We utilize the Stefan Boltzmann distribution to generate the partons, or Jüttner distribution to generate the hadrons, considering the strangeness suppression and mass difference in the phase transition. We give the ratio of generated parton types in equilibrium state with considering the quark masses via the strangeness suppression factor *e.g.* $\gamma_s = 0.3$, according to the mass difference of the light quarks and strange quarks at an average transition temperature. Of course, this ratio also affects the momentum distribution for different parton types.

(4) The 4-momenta of the particles are generated according to the Cooper-Frye formula [30]. The baryon chemical potentials for the given baryon number densities are taken into account. As we mentioned above, we are choosing a time step ($t = \text{Constant}$), and dispersing the partons into the fluid cells with proper distributions after the hyper-surface.

These steps are done for all fluid cells of the hydro code, which are carrying baryon number density, pressure and momentum. The created partons serve as parton initialization for the PACIAE model.

III. ASSESSMENT IN ULTRARELATIVISTIC HEAVY ION COLLISIONS

Figures 1 and 2 show the velocity and temperature change in the transition from the QGP fluid to partonic matter as function of the energy density for different transition time steps, 3.8 fm/c and 5.0 fm/c, in the Hydro-PACIAE hybrid model calculation. We can see that the cell by cell changes from the QGP fluid to partonic matter are modest except at low energy densities where the velocity and temperature change visibly.

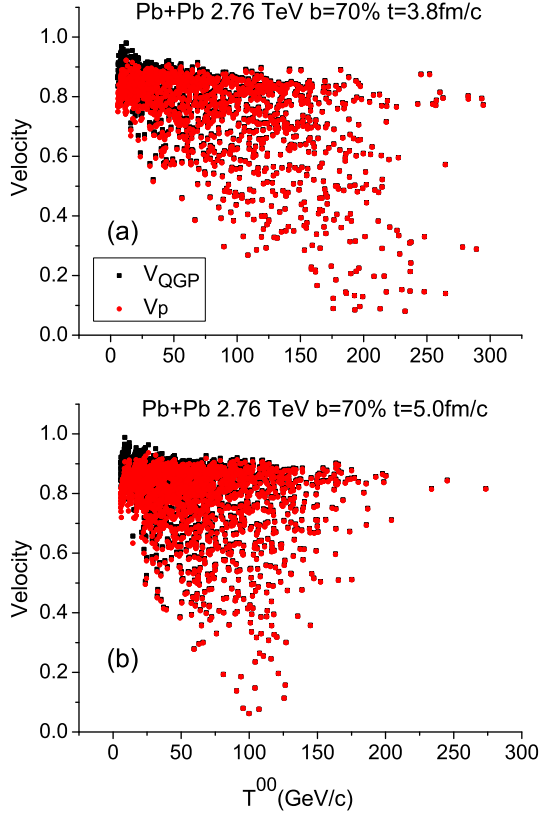


FIG. 1: Velocity change in the transition as function of the energy density in different transition time steps, (a) 3.8 fm/c and (b) 5.0 fm/c, in the Hydro-PACIAE hybrid model calculation. The cell by cell changes from the QGP (black squares) to the partonic matter (red dots) are modest except at low energy densities where the velocity visibly decreases.

For comparing the results of Hydro-PACIAE hybrid model with the results of Hydro code conveniently, we calculated the Au+Au collisions at $\sqrt{s_{NN}}=130$ GeV. The final charged particle pseudo-rapidity distribution is shown in Fig. 3, where the calculated results of Hydro-PACIAE model is compared with the PHOBOS data [31]. The observed centrality bins correspond to a set of impact parameters, which yield to different multiplicities depending on the impact parameter and the FO time. This is illustrated in Ref. [19] for the case of Pb+Pb reactions at LHC energy, and the dependence is similar at lower energies also. In the FD model the calculated charged particle multiplicity, N_{ch} , is a function of FO time (assuming a $t_{FO} = const.$ FO hyper-surface), and of the impact parameter, b . These multiplicities can be matched to the measured mean charged multiplicity in a given experimental multiplicity bin. For example, the impact parameter $b = 5.5$ fm for Au+Au collisions corresponds approximately to the experimental centrality of 20% and $b = 8.2$ fm for centrality of 40%. This is similar to the impact parameter method in transport model [32].

We also calculated the transverse momentum distribu-

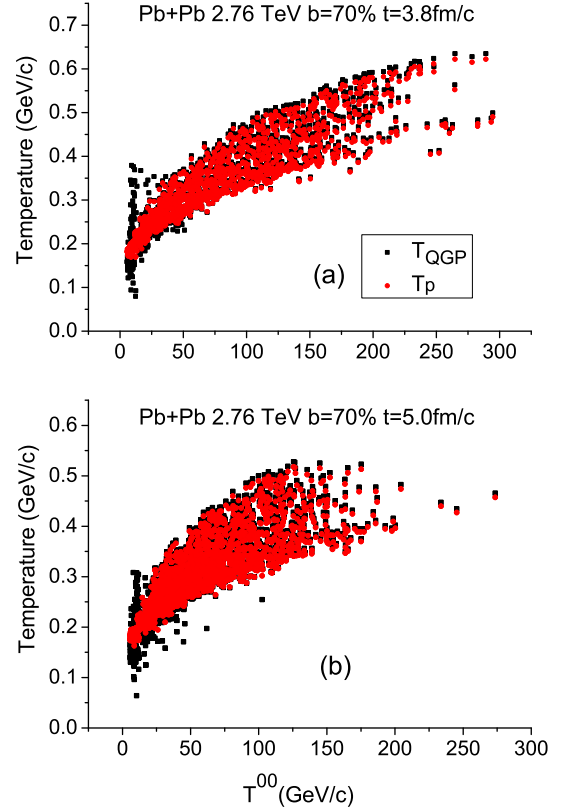


FIG. 2: Temperature change in the transition as function of the energy density in different transition time steps, (a) 3.8 fm/c and (b) 5.0 fm/c, in the hybrid model calculation. The cell by cell changes from the QGP (black squares) to the partonic matter (red dots) are modest except at low energy densities where the temperature slightly increases and becomes more concentrated.

tion for the Au+Au collisions at $\sqrt{s_{NN}}=130$ GeV and compared the results with the STAR data[33] in Fig. 4. The good agreement in Figs. 3 and 4 indicate that our Hydro-PACIAE hybrid model can successfully reproduce the experiment data at RHIC energy.

Figure 5 shows the pseudo-rapidity distribution of Hydro-PACIAE hybrid model for the Pb+Pb collisions at $\sqrt{s_{NN}}=2.76$ TeV together with the CMS data, which are taken from [34] and the pseudo-rapidity range is from -2.5 to 2.5. We can see that in the $|\eta| < 2.5$ area, the hybrid model results are well compared with the CMS data. The transverse momentum distribution for the Pb+Pb collisions at $\sqrt{s_{NN}}=2.76$ TeV are also calculated and the results are shown in Fig. 6 compared with the ALICE data [35]. We can see that in the low and middle p_T regions the hybrid model results well reproduce the ALICE data, but the model results are smaller in the high p_T region.

We used the Hydro-PACIAE hybrid model to calculate the elliptical flow for the Pb+Pb collisions at $\sqrt{s_{NN}}=2.76$ TeV. The results are compared with the AL-

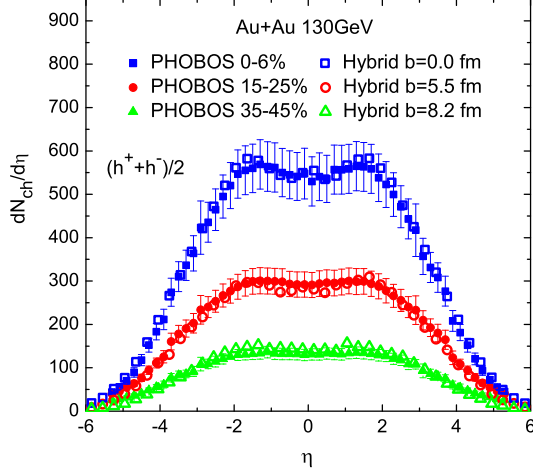


FIG. 3: Charged particle pseudo-rapidity distribution from the Hydro-PACIAE hybrid model calculations, and PHOBOS data [31] in Au+Au collisions at $\sqrt{s_{NN}}=130$ GeV. The experimental data are given in the indicated centrality bins (full symbols) and for these the corresponding mean impact parameters (open symbols) are indicated for the hybrid model calculations.

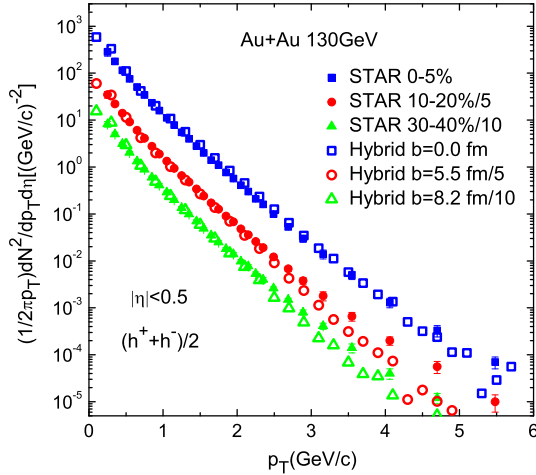


FIG. 4: p_T distribution for the Hydro-PACIAE hybrid model calculation and STAR data [33] in Au+Au collisions at $\sqrt{s_{NN}}=130$ GeV, for the same centrality bins and mean impact parameters as in Figure 3.

ICE data[36, 37] in Fig. 7. We see that in the low p_T region the Hydro-PACIAE hybrid model results are smaller than the ALICE data, but the model results are bigger than the ALICE data for the high p_T region. This feature originates from the hydro model [19], mainly because the Hydro code in the Hydro-PACIAE hybrid model is

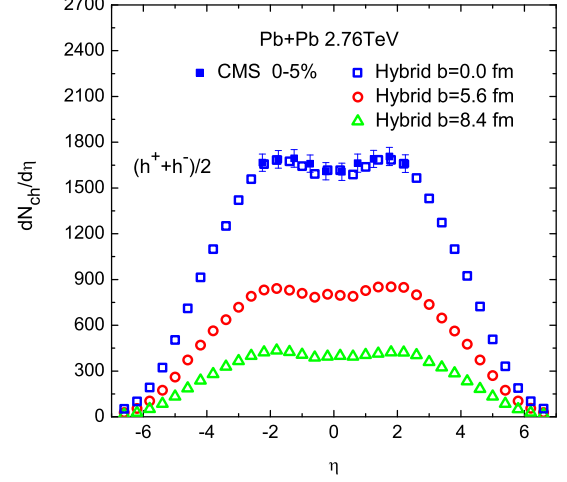


FIG. 5: Charged particle pseudo-rapidity distribution from the Hydro-PACIAE hybrid model calculations, and CMS data [34] in central collisions. The experimental data are given in the indicated centrality bin (full symbols) and the mean impact parameters (open symbols) are indicated for the hybrid model calculations.

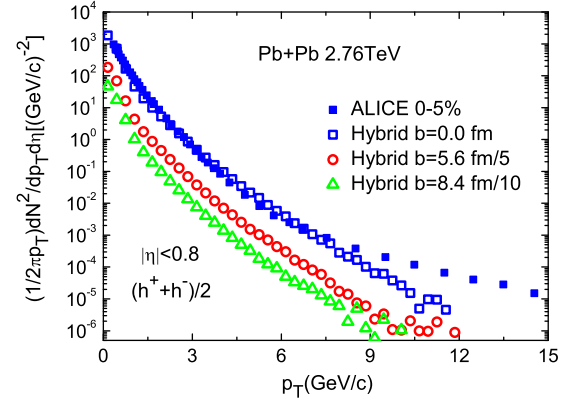


FIG. 6: p_T distribution for the Hydro-PACIAE hybrid model calculation, and ALICE data [35] in central collisions, for the same centrality bin and mean impact parameters as in Figure 5.

ideal fluid dynamics and has little viscosity. The FO time is also an important quantity for the elliptical flow. We compared the v_2 with different FO time evolution for 40% centrality Pb+Pb collisions at $\sqrt{s_{NN}}=2.76$ TeV in Fig. 8. The v_2 value becomes bigger when the Hydro evolution time increases from 0.423 to 2.54 and 5.08 fm/c. This is because when the Hydro evolution time is longer more elliptic flow develops with time in the Hydro-PACIAE hybrid model.

The directed flow, $v_1(\eta)$ for Pb+Pb collisions at $\sqrt{s_{NN}}=2.76$ TeV was also evaluated in the hybrid model,

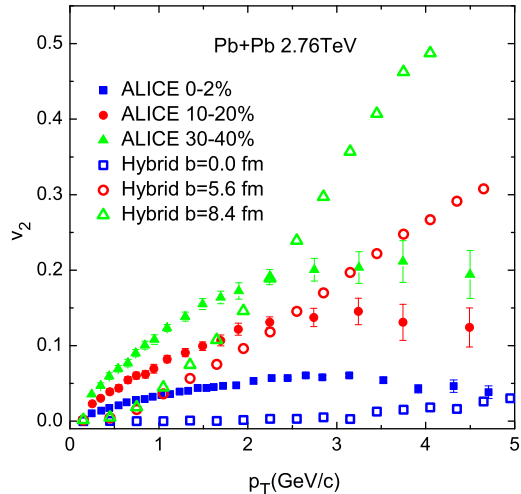


FIG. 7: v_2 distribution for the Hydro-PACIAE hybrid model calculation, and ALICE data in central collisions and semi central collisions, for the same centrality bins and mean impact parameters as in Figure 5. The 0-2% ALICE data are taken from [36], and 10-20%, 30-40% are taken from [37].

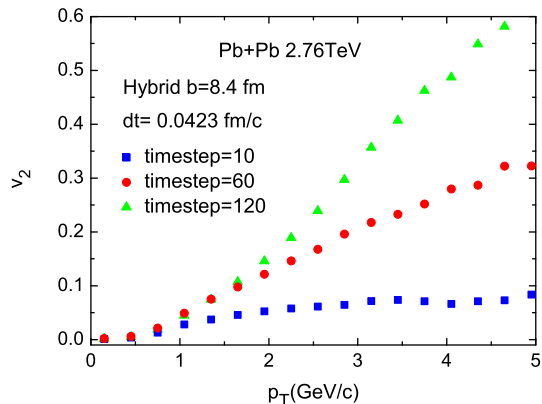


FIG. 8: v_2 distribution for the Hydro-PACIAE hybrid model calculation with different time step evolution.

for centrality percentage bins 40% and 60%. The obtained $v_1(\eta)$ showed a random statistical fluctuation around zero with a $v_1(\eta)$ -amplitude of 0.1% for $|\eta| < 4$, which increased to 0.2% for $|\eta| > 4$, due to the smaller charged particle multiplicity at higher pseudorapidities. The obtained $v_1(p_T)$ was zero at low p_T and reached to 1% (3%) at $p_T = 3(4)$ GeV/c respectively due to statistical fluctuations with decreasing charged particle multiplicity. Thus, the fluctuations arising from the transport model PACIAE, dominated the smaller azimuthal asymmetry, $v_1(\eta)$, from the initial FD stage of the hybrid model. The same situation was observed for $v_1(p_T)$, where the FD expectation for global collective flow van-

ishes due to symmetry reasons.

The elliptic flow, $v_2(\eta)$ was also dominated by strong statistical fluctuations. Both for the directed and elliptic flow the reaction plane of the evaluation was the theoretical reaction plane given by the impact parameter vector. The initial states, arising from the FD stage of the model did not include any random fluctuation. These results are consistent with the experimental finding that the central and semi-central collisions are dominated by random fluctuations, especially by random initial state fluctuations, which are not correlated with the reaction plane.

IV. CONCLUSIONS

Combining the hydrodynamic model (Hydro code) and the transport model (PACIAE model), we have presented the Hydro-PACIAE hybrid model. We used the Hydro-PACIAE hybrid model to calculate Au+Au collisions at $\sqrt{s_{NN}}=130$ GeV and Pb+Pb collisions at $\sqrt{s_{NN}}=2.76$ TeV. The pseudo-rapidity and transverse momentum distributions well reproduce the experimental data. This shows that the Hydro-PACIAE hybrid model is effective to describe the ultrarelativistic Heavy Ion Collisions at RHIC and LHC Energies. We used the hybrid model to calculate the elliptical flow for the Pb+Pb collisions at $\sqrt{s_{NN}}=2.76$ TeV. The v_2 values are bigger than the experimental data in the high p_T region, and it shows that the v_2 value will become bigger when the Hydro evolution time is longer. This result indicates significant dependence on the choice of the transition surface between the two components of the hybrid model. Furthermore, the space-time shape of the FO surface may also influence the final anisotropy produced by the model.

The fluid dynamical model needs an initial stage of relativistic heavy ion collisions to start, and the so-called Effective String Rope model was used to generate the initial stage for Hydro code [11, 12]. We also plan to use the transport model, PACIAE, to generate the initial stage for Hydro code instead of the Effective String Rope model. Then we will present a full transport model with an intermediate hydrodynamic stage to study the relativistic heavy ion collisions. The variability of the model components, will enable us a bigger flexibility to study the role of different model assumptions, initial state and transition conditions on a wide set of observables.

V. APPENDIX

A. The transition procedure

Here we evaluate and present the details of the transition from the FD stage to the parton cascade stage of the model in case of a $t = \text{Constant}$ transition hypersurface. All components of the energy momentum tensor of the QGP are described in the PIC hydrodynamic model.

The hydro code uses the Bag Model EoS with $N_F = 2$. However, some of the fluid cells with low internal energy would have negative pressures due to the Bag constant, which are set to zero in the model. Thus, we need to calculate the conserved quantities in the transition from QGP to partonic matter both for the cases of positive and zero pressure. First, in the QGP phase, the energy density component and momentum current component, as well as the baryon charge current are as follows:

$$T_{QGP}^{00} = (e_{QGP} + P_{QGP})\gamma_{QGP}^2 - P_{QGP} = e_{cf} \quad (4)$$

$$T_{QGP}^{10} = (e_{QGP} + P_{QGP})\gamma_{QGP}^2 v_{QGP} \quad (5)$$

$$N_{QGP}^0 = n_{QGP}\gamma_{QGP} \quad (6)$$

where e_{cf} is the energy density in the QGP phase in the calculational frame (CF). In the general case, when the 3-velocity of the fluid is directed arbitrarily, $\vec{v}_{QGP} = (v_{QGP-x}, v_{QGP-y}, v_{QGP-z})$, which is known from the hydro code, then the parton side flow will keep the velocity *3-direction* in each cell because we assumed that the transition happens at a $t = \text{Constant}$ hyper-surface. Then after transition the velocity relationship between the pre- and post- transition velocities can be written as:

$$v_x^P = \frac{v_x^{QGP}}{|\vec{v}_{QGP}|} v_P, \quad v_y^P = \frac{v_y^{QGP}}{|\vec{v}_{QGP}|} v_P, \quad v_z^P = \frac{v_z^{QGP}}{|\vec{v}_{QGP}|} v_P$$

Here $|\vec{v}_{QGP}| = \sqrt{v_x^2 + v_y^2 + v_z^2}$ in the QGP phase and the r.h.s quantities are known from hydro code. On the parton side, we have

$$\gamma_P^2 = \frac{1}{1 - v_P^2}, \quad \text{or} \quad v_P = \sqrt{\frac{\gamma_P^2 - 1}{\gamma_P^2}},$$

and we use the EoS in the QGP phase:

$$e_{QGP} + P_{QGP} = 4(P_{QGP} + B_{bag})$$

a. Positive pressure in fluid cells: When the fluid cells have positive pressure, based on Eqs. (4), (5) and using the EoS, we can obtain P_{QGP} and e_{QGP} , which are expressed by the known e_{cf} , and v_{QGP} (γ_{QGP}) as:

$$P_{QGP} = \frac{e_{cf} - 4B_{bag}\gamma_{QGP}^2}{4\gamma_{QGP}^2 - 1} \quad (7)$$

$$e_{QGP} = \frac{3e_{cf} + 4B_{bag}\gamma_{QGP}^2 v_{QGP}^2}{4\gamma_{QGP}^2 - 1}. \quad (8)$$

Inserting these into the Eqs. (4) and (5), we get the conserved quantities T^{00} and T^{10} in terms of e_{cf} and v_{QGP} as:

$$T_{QGP}^{00} = e_{cf}$$

$$T_{QGP}^{10} = \frac{4\gamma_{QGP}^2 v_{QGP}}{4\gamma_{QGP}^2 - 1} (e_{cf} - B_{bag})$$

b. Zero pressure in fluid cells: In this case, we use the general definition, Eqs. (4) and (5) with the condition $P_{QGP} = 0$ for these fluid cells, and we obtain the simple expressions:

$$T_{QGP}^{00} = e_{cf}$$

$$T_{QGP}^{10} = e_{cf} v_{QGP}.$$

This is necessary because in these cells with zero pressure, we do not use the MIT Bag model EoS, and the relation between T^{00} and T^{10} should be consistent with the modification.

B. Solving the conservation laws

The transition from QGP to partonic phase have to satisfy the conservation laws, Eq. (1), and the solution of this boundary condition is done in [10]. Here we defined the conserved energy momentum current, \mathbf{A}^μ ,

$$\mathbf{A}^\mu \equiv T^{\mu\nu} d\sigma_\nu = w u^\mu u^\nu d\sigma_\nu - P g^{\mu\nu} d\sigma_\nu,$$

and the baryon current j ,

$$j \equiv N^\mu d\sigma_\mu = n u^\mu d\sigma_\mu. \quad (9)$$

With the notation, $w = e + P$, the above two quantities are a 4-vectors and an invariant scalar, which can be considered as crossing the hyper-surface element, moreover, we construct two invariant scalar equations of the conserved energy momentum current by (i) taking its norm, $\mathbf{A}^\mu \mathbf{A}_\mu$, and (ii) taking its projection to the normal direction, $\mathbf{A}^\mu d\sigma_\mu$, they have the expressions as:

$$\mathbf{A}^\mu \mathbf{A}_\mu = w(e - P)(u^\mu d\sigma_\mu)^2 + P^2(d\sigma^\mu d\sigma_\mu), \quad (10)$$

$$\mathbf{A}^\mu d\sigma_\mu = w(u^\mu d\sigma_\mu)^2 - P(d\sigma^\mu d\sigma_\mu). \quad (11)$$

Eliminating the term $w(u^\mu d\sigma_\mu)^2$ from Eqs. (10) and (11), we obtain that

$$\mathbf{A}^\mu \mathbf{A}_\mu = (e - P)\mathbf{A}^\mu d\sigma_\mu + e P (d\sigma^\mu d\sigma_\mu). \quad (12)$$

In the same way, put Eq. (9) into Eq. (11), then we get

$$j^2 \frac{w}{n^2} = \mathbf{A}^\mu d\sigma_\mu + P(d\sigma^\mu d\sigma_\mu) \quad (13)$$

Thus if we know the pre transition $T_{QGP}^{\mu\nu}$ and $d\sigma_\mu$, we can get the solution from Eqs. (12) and (13) to obtain the post transition configuration, with the equation of state. For example, using the simplest case in our simulation, where the post transition EoS is simply $P_P = E_P/3$, then from Eq. (12) we get,

$$d\sigma^\mu d\sigma_\mu E_P^2 + 2\mathbf{A}^\mu d\sigma_\mu E_P - 3\mathbf{A}^\mu \mathbf{A}_\mu = 0, \quad (14)$$

and if we assume $d\sigma^\mu = (1, 0, 0, 0)$ and $u^\mu = \gamma(1, v_{QGP}, 0, 0)$, then

$$\mathbf{A}^\mu \mathbf{A}_\mu = (T_{QGP}^{00})^2 - (T_{QGP}^{10})^2 \quad \text{and} \quad \mathbf{A}^\mu d\sigma_\mu = T_{QGP}^{00},$$

and then E_P can be solved from the quadratic Eq. (14) with the help of Eqs. (4) and (5). In the same way, we can solve n_P from Eq. (9), together with Eq. (13).

Acknowledgements

This work was supported by the National Natural Science Foundation of China under Grants No. 11105227, 11175070, 11075217, 11047142, 10975062 and the 111

project of the foreign expert bureau of China. Dr. Yu-liang Yan and Yun Cheng thank for the kind hospitality from Prof. L.P Csernai of the Institute for physics and technology, University of Bergen, where part of this work was done.

-
- [1] I. Arsene, et al., BRAHMS Collaboration, Nucl. Phys. A **757**, 1 (2005).
 - [2] B.B. Back, et al., PHOBOS Collaboration, Nucl. Phys. A **757**, 28 (2005).
 - [3] J. Admas, et al., STAR Collaboration, Nucl. Phys. A **757**, 102 (2005).
 - [4] K. Adcox, et al., PHENIX Collaboration, Nucl. Phys. A **757**, 184 (2005).
 - [5] H. Petersen, J. Steinheimer, G. Burau, M. Bleicher, and H. Stöcker, Phys. Rev. C **78**, 044901 (2008).
 - [6] S.A. Bass, A. Dumitru, M. Bleicher, L. Bravina, E. Zabrodin, H. Stöcker, and W. Greiner, Phys. Rev. C **60**, 021902 (1999).
 - [7] T. Hirano, P. Huovinen, Y. Nara, arXiv:1012.3955v1 [nucl-th].
 - [8] B. Bauchle and M. Bleicher, Phys. Rev. C **81**, 044904 (2010).
 - [9] B. Abelev, arXiv:1109.4185v1 [hep-ph]
 - [10] Yun Cheng, L. P. Csernai, V.K. Magas, B.R. Schlei, and D. Strottman, Phys. Rev. C **81**, 064910 (2010).
 - [11] V.K. Magas, L.P. Csernai and D.D. Strottman, Phys. Rev. C **64**, 014901 (2001).
 - [12] V.K. Magas, L.P. Csernai and D.D. Strottman, Nucl. Phys. A **712**, 167 (2002).
 - [13] K. Aamodt et al., (ALICE Collaboration) Phys. Rev. Lett. **105**, 252302 (2010).
 - [14] P.K. Kovtun, D.T. Son and A.O. Starinets, Phys. Rev. Lett. **94**, 111601 (2005).
 - [15] L.P. Csernai, J.I. Kapusta, L.D. McLerran, Phys. Rev. Lett. **97**, 152303–4 (2006).
 - [16] Martha W. Evans, Francis H. Harlow, The Particle In Cell Method for Hydrodynamic Calculations, Los Alamos Scientific laboratory, (1957)
 - [17] L.P. Csernai, and J.I. Kapusta, Phys. Rev. Lett. **69**, 737 (1992); and L.P. Csernai, and J.I. Kapusta, Phys. Rev. D **46**, 1379 (1992).
 - [18] L.P. Csernai, Y. Cheng, V.K. Magas, I.N. Mishustin, and D. Strottman, Nucl. Phys. A **834**, 261c (2010).
 - [19] L.P. Csernai, V.K. Magas, H. Stöcker, and D.D. Strottman, Phys. Rev. C **84**, 024914 (2011), arXiv: 1101.3451 v1-3 [nucl-th].
 - [20] Sz. Horvat, V.K. Magas, D.D. Strottman, L.P. Csernai, Phys. Lett. B **692**, 277 (2010).
 - [21] Yu-Liang Yan, Dai-Mei Zhou, Bao-Guo Dong, Xiao-Mei Li, Hai-Liang Ma, and Ben-Hao Sa, Phys. Rev. C **79**, 054902 (2009); arXiv: 0903.0915 v2 [nucl-th].
 - [22] Yun Cheng, Yu-Liang Yan, Dai-Mei Zhou, Xu Cai, Ben-Hao Sa, and Laszlo P. Csernai, Phys. Rev. C **84**, 034911 (2011).
 - [23] Ben-Hao Sa, Dai-Mei Zhou, Yu-Liang Yan, Xiao-Mei Li, Sheng-Qin Feng, Bao-Guo Dong, and Xu Cai, arXiv: 1104.1238 v1 [nucl-th].
 - [24] T. Sjöstrand, Comput. Phys. Commun. **82**, 74 (1994).
 - [25] P. Csizmadia and P. Levai, Phys. Rev. C **61**, 031903 (2000).
 - [26] R.J. Fries, B. Muller, C. Nonaka, and S.A. Bass, Phys. Rev. Lett. **90**, 202303 (2003)
 - [27] B.L. Combridge, J. Kripfgang, and J. Ranft, Phys. Lett. **70**, 234 (1977).
 - [28] P. Koch, B. Müller, and J. Rafelski Phys. Rep. **142**, 167 (1986).
 - [29] A. Baldini, et al., “Total cross sections for reactions of high energy particles”, Springer-Verlag, Berlin, 1988.
 - [30] F. Cooper, G. Frye, Phys. Rev. D **10** (1974) 186.
 - [31] B.B. Back, et al., PHOBOS Collaboration, Phys. Rev. Lett. **87**, 102303 (2001).
 - [32] Ben-Hao Sa, A. Bonasera, An Tai, and Dai-Mei Zhou, Phys. Lett. B **537**, 268 (2002).
 - [33] C. Adler, et al., STAR Collaboration, Phys. Rev. Lett. **89**, 202301 (2002).
 - [34] S. Chatrchyan, et al., CMS Collaboration, JHEP **08**, 141 (2011); arXiv: 1107.4800v1 [nucl-ex].
 - [35] K. Aamodt, et al., ALICE Collaboration, arXiv: 1012.1004v1 [nucl-ex].
 - [36] K. Aamodt, et al., ALICE Collaboration, Phys. Rev. Lett. **107**, 032301 (2011); arXiv: 1105.3865v2 [nucl-ex].
 - [37] K. Aamodt, et al., ALICE Collaboration, arXiv: 1106.1341v1 [nucl-ex].